



# Production of Nickel by Cold Hydrogen Plasma: Role of Active Oxygen

Kali Charan Sabat<sup>1</sup>

Received: 8 July 2021 / Accepted: 22 March 2022 / Published online: 13 April 2022

© The Author(s), under exclusive licence to Springer Science+Business Media, LLC, part of Springer Nature 2022

## Abstract

A new cold hydrogen plasma (CHP) technology for producing various metals and alloys from their oxides/ores has been recently introduced. CHP generates excited species, which lower the thermodynamic and kinetic barriers to reduction, making the reduction of metal oxides/ores easier and faster. Among the metal oxides, nickel (Ni) could be produced very quickly from nickel oxide (NiO), as reported in a recent publication (<https://doi.org/10.1007/s11090-021-10194-3>). The presence of excess or active oxygen was ascribed to the faster reduction. For the reduction of metal oxides, thermodynamics and kinetics are well-known reduction pathways. However, the influence of active oxygen on thermodynamics and kinetics was never reported before. As a result, the purpose of the study was to investigate the effect of active oxygen on the thermodynamics and kinetics of NiO reduction. The active oxygen in NiO has been found to increase the thermodynamic potential by significantly lowering the Gibbs standard free energy by a significant amount. Further, it also decreases the NiO bond stability. The active oxygen also provides kinetic advantage by creating more area for diffusion. These characteristics accelerate the NiO reduction to the point where a  $7.5 \times 10^{-6}$  kg pellet could be reduced in 1200 s using 600 W microwave power and a hydrogen flow rate of  $1.166 \times 10^{-6}$  m<sup>3</sup> s<sup>-1</sup>, opening the possibility of NiO reduction by CHP to be scaled up.

**Keywords** Active oxygen · Thermodynamics · Reaction kinetics Nickel production · Cold hydrogen plasma · Gibbs standard free energy

## Introduction

Recently, cold hydrogen plasma (CHP) could extract metals such as iron (Fe), copper (Cu), Cobalt (Co), Nickel (Ni) from their oxides/ores. Alloys like FeCo, CuCo, CuNi, etc., could also be produced from the reduction of mixtures of their oxides. Nickel being a strategically important metal, the production of Ni by CHP has been reported in the most recent publication (<https://doi.org/10.1007/s11090-021-10194-3>). Ni is primarily extracted from

---

✉ Kali Charan Sabat  
kcsabat@gmail.com; drkcsabat@manit.ac.in

<sup>1</sup> Department of Materials and Metallurgical Engineering, Maulana Azad National Institute of Technology, Bhopal, Madhya Pradesh 462003, India

oxide ores [1–6], with variation in composition and mineralogy [7–10]. Because of these wide variations, a standard extraction flow sheet cannot be used for Ni; as a result, Ni is extracted from different ores using separate methods, by using pyrometallurgical, hydrometallurgical, or a combination of the two [11]. Intermediate products are formed during the processing routes. NiO is one of them. Several reductants have been used to extract Ni from NiO [6, 9, 12–29]. Hydrogen ( $H_2$ ) is the most favorable among these reductants due to its environmental friendliness, quicker reduction kinetics, and ability to generate pure Ni without other contaminants. [30–33]. Although  $H_2$  has many advantages, it has thermodynamic restriction due to the smaller negative value of the Gibbs standard free energy ( $\Delta G$ ) of NiO—Ni reduction. Also, there are several kinetic constraints, such as induction period [34–37] and more than one order variation of activation energy [21, 38–42] ranging from 10 to 137 kJ/mol. Furthermore, there are limitations in modelling this reduction reaction; around 20 kinetic models [21, 38–40, 43–50] have been developed, none have gained wide adoption. Various factors, such as temperature and pressure, which impact the rate of  $H_2$  diffusion, have been ascribed for the wide variations of the above kinetic constraints. Sample size, shape, and composition are further parameters that affect lattice strain and thus the reduction kinetics. Richardson et al. [43] attributed additional factors such as porosity, powder size, water ( $H_2O$ ) molecules, etc. Although it is widely understood that NiO is a p-type non-stoichiometric oxide with excess/active oxygen, the influence of active oxygen on the rate of hydrogen reduction of NiO was not documented. However, recently, active oxygen has been reported to enhance the reduction of NiO significantly [51]. The author observed that NiO contains active oxygen, which helps CHP to reduce NiO  $\rightarrow$  Ni faster. However, the percentage reduction exceeded 100% due to the extra oxygen, making kinetic laws challenging to apply.

Nevertheless, using the same CHP, rate laws could be successfully applied to extract several metals and alloys from their oxides [51–57] or oxide mixtures [57–60], respectively. From these experimental results, CHP is found to be successful in overcoming the thermodynamic and kinetic restrictions of  $H_2$ . There were no problems in estimating percentage reductions from weight loss of oxygen or applying the rate equations in these investigations. However, while reducing NiO, the percentage reduction consistently exceeded 100%. This problem could not be avoided, despite extensive efforts to avoid oxygen absorption. The application of rate laws became complicated by the presence of too much oxygen, prompting the current research. The following factors influenced the decision to conduct this study: (a) NiO  $\rightarrow$  Ni reduction is a unit step in the Ni extraction flow sheet, (b) the estimated percentage reduction of NiO exceeded 100%, (c) a significant amount of active oxygen is present in NiO, (d) the active oxygen has been found to enhance the NiO  $\rightarrow$  Ni reduction, (e) application of rate laws are difficult to apply in the presence of active oxygen, (f) the effect of active oxygen on NiO  $\rightarrow$  Ni reduction has not been reported.

## Experimental Details

The CHP's experimental specifics, including the production of compressed pellets from metal oxide powders, the experimental set-up, and the experimental methodology, have been addressed in previous papers [51–53, 61]. The pellets used in this investigation were cylindrical (diameter:  $20 \times 10^{-3}$  m, height:  $2 \times 10^{-3}$  m to  $6 \times 10^{-3}$  m). They were put on a molybdenum pellet holder placed at the center of the microwave oven. Imagine heating food in one of our domestic microwave ovens to get a sense of the reduction chamber. The

reduction chamber is sealed after keeping the pellet inside the chamber. To eliminate any unwanted gaseous species, the chamber is evacuated to a pressure of 0.1 Pa. The H<sub>2</sub> is then delivered into the reduction chamber at the experiment's set flow rate. The microwave is turned on after the chamber pressure reaches 666 Pa. Microwaves at a frequency of  $2.45 \times 10^9 \text{ s}^{-1}$  are produced in the reduction chamber. The polarity of the H<sub>2</sub> molecules interacts with the microwave's high-frequency electromagnetic field. As a result, H<sub>2</sub> becomes excited, resulting in excited species that comprise the CHP. Microwave power and chamber pressure control the CHP. CHP interacts with the pellet, and reduction begins at the surface of the pellet where CHP interacts. The heat produced during reduction at the CHP-pellet reduction interface causes the reduction. The reactor receives no additional internal or external heating [54, 57–59, 62].

The powders of NiO and CuO used in the current investigation have already been reported earlier [51, 62]. Phase analysis was used to characterize the NiO powders using X'Pert PRO-PANalytical (Model Number—3040160) and JCPDS file no JCPDS-00-047-1049. Similarly, CuO was characterized.

Temperature, pressure, H<sub>2</sub> flow rate, microwave power, and other parameters were carefully monitored during the tests. After completing the experiment, the weight loss during reduction was estimated using a computerized weighing balance with an accuracy of  $0.1 \times 10^{-6} \text{ kg}$ . To assess the active oxygen, wet chemical analysis (iodometry) and electron spectroscopy for chemical analysis (ESCA) or X-ray photoelectron spectroscopy (XPS) were utilized. The PHI ESCA model 5600 spectrometer was used to measure the XPS spectra of O(1 s) core level over an area of  $800 \times 10^{-6} \text{ m}$  diameter using Al K $\alpha$  X-ray, with an excitation power of 300 W and a pass energy of 150 eV. Shirley's background was removed as the baseline from the O(1 s) spectra. A blend of Gaussian and Lorentzian functions was used to fit the least-square curve, with a Gaussian percentage exceeding 80%.

## Results and Discussion

Reduction studies of NiO and CuO pellets were carried out with small NiO pellets ( $\sim 2.5 \times 10^{-3} \text{ kg}$ ). The pellets were cylindrical with a diameter of  $2 \times 10^{-2} \text{ m}$ . This size was also investigated in earlier studies [51, 54, 57–59, 62]. However, the size was increased up to  $\sim 7.5 \times 10^{-3} \text{ kg}$ . The results of the reduction studies are shown in Table 1. Only a few experimental results have been provided here because the percentage reductions exceeded 100%. The experimental result of the same sized CuO pellet reduced under the same

**Table 1** Percentage reduction obtained from weight loss (oxygen loss)

Samples	Power/W	Flow rate/ $\times 10^{-6} \text{ m}^3 \text{ s}^{-1}$	Time/s	Initial weight/ $10^{-3} \text{ kg}$	Final weight/ $10^{-3} \text{ kg}$	Percentage reduction/weight loss
CuO[62]	750	2.500	1200	2.490	1.978	102
NiO	750	2.500	300	2.512	1.904	113
NiO	750	1.166	300	2.492	1.931	105
NiO	750	3.333	300	2.522	1.860	123
NiO	600	1.166	1200	7.642	6.086	95

operating parameters is provided for comparison. The details of reduction of CuO by CHP, with nucleation growth kinetics, have already been reported elsewhere [62].

The percentage reductions were estimated from the ratio of weight loss (i.e., initial mass–instantaneous mass) to the stoichiometric amount of oxygen in CuO and NiO samples, as done in earlier investigations [52–54, 58, 59, 62]. The stoichiometric amount is the quantity of oxygen estimated from the chemical formula CuO and NiO. As shown in Table 1, under the same plasma operating parameters for  $\sim 2.5 \times 10^{-3}$  kg pellet, CuO reduces completely to Cu in 1200 s. The estimated percentage of reduction is 102%. The extra 2% might be due to some measurement errors or due to moisture adsorption of CuO from the ambient atmosphere [63]. However, the other percentage reductions reported for the reduction of CuO never exceeded 100% [62]. In contrast, the percentage reduction obtained from NiO goes up to 123%. Like this, several percentages exceeded 100%, as shown in Table 1 and the earlier publication [51].

Due to the repeated results of more than 100% reduction obtained from the weight loss calculation in the earlier paper [51], the percentage reduction was also determined by quantitative XRD by Rietveld analysis, which yielded an appropriate percentage estimation. Nevertheless, the recurrent results of more than 100% reduction and difficulty in applying rate laws gave rise to the issue of active oxygen in NiO. The amount of active oxygen is mostly dependent on the processing method. This extra oxygen comes from two places: (a) chemisorbed oxygen on the surface (also known as surface active oxygen) and (b) active oxygen in the lattice (called lattice active oxygen) [64]. The total of these two has been called active oxygen. The majority of active oxygen comes from the surface active oxygen, which is easily removed compared to the lattice active oxygen [64].

## Estimation of Active Oxygen in NiO

### XRD Analysis

The XRD of raw materials NiO and CuO are shown in Fig. 1 and Fig. 2. The final reduction products are Ni and Cu, shown in Fig. 3 and Fig. 4, respectively.

The XRD of the raw NiO sample was carried out with a molybdenum target and identical XRD settings [51, 52, 54, 57–59, 62] over a  $2\theta$  range of 10–47° (Fig. 1). The NiO

**Fig. 1** XRD of the raw NiO used for the investigation [51]. Reproduced with permission from Springer

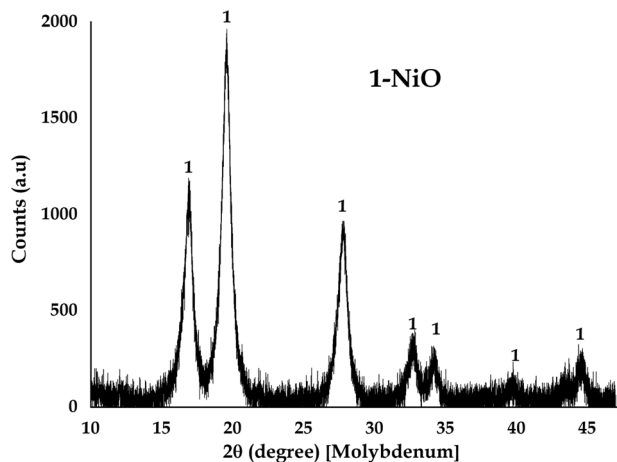


**Fig. 2** XRD of the raw CuO used for the investigation [62]. Reproduced with permission from Springer

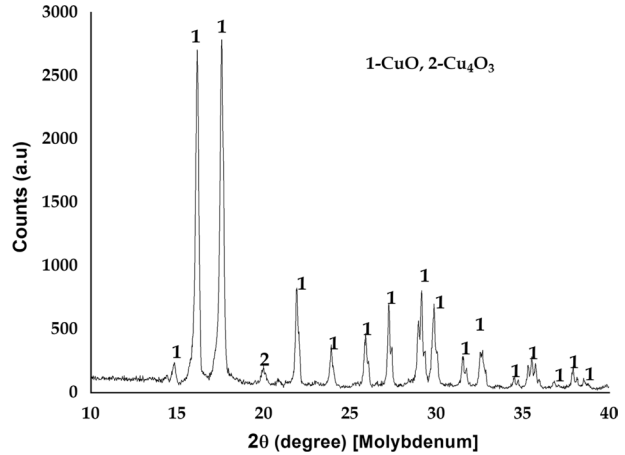


**Fig. 3** XRD pattern of the reduction product (Nickel) at pellet size  $2.512 \times 10^{-3}$  kg, hydrogen flowrate  $2.500 \times 10^{-6}$  m<sup>3</sup> s<sup>-1</sup>, microwave power 750 W

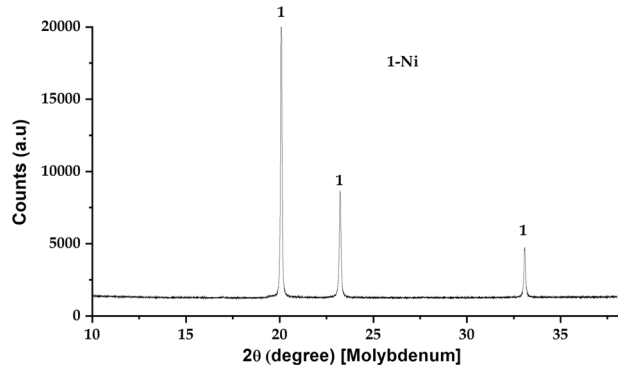
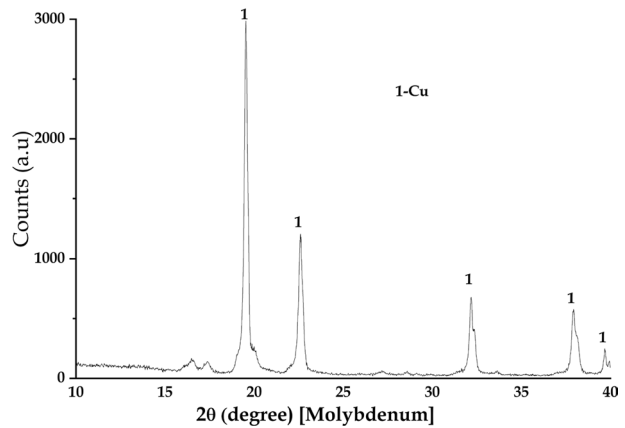


**Fig. 4** XRD pattern of the reduction product (Copper) at pellet size  $2.490 \times 10^{-3}$  kg, hydrogen flow rate  $2.500 \times 10^{-6}$  m<sup>3</sup> s<sup>-1</sup>, microwave power 750 W



powder is pure, with no Ni or its oxides present. Similarly, XRD of CuO was also done with the same molybdenum target over a  $2\theta$  range of 10–40° (Fig. 2). The CuO was also found to be pure with traces of Cu<sub>4</sub>O<sub>3</sub> [80]. The XRD of NiO (Fig. 1) shows huge

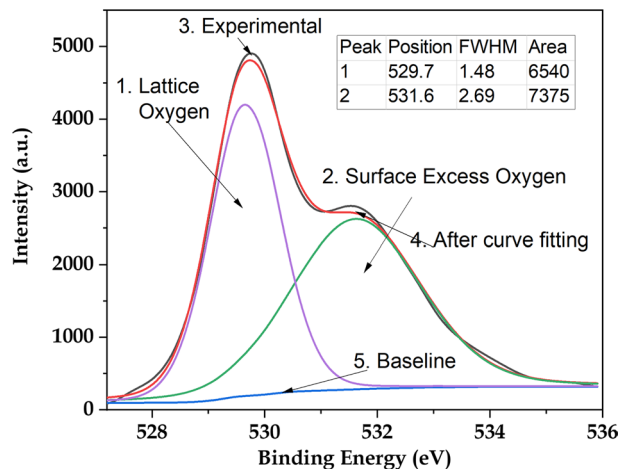
fluorescence in the XRD background, whereas XRD of CuO (Fig. 2) showed only marginal noise. The noise difference between the NiO and CuO is attributable to a variation in stoichiometry. CuO is stoichiometric, whereas NiO is non-stoichiometric. The background noise in the XRD of NiO couldn't be avoided even after changing the target material to copper and carrying out the XRD at a long scan time (80 s) using a small step size ( $0.0170^\circ$ ) [51]. The background noise was attributed to the considerable number of defects (i.e., surface active oxygen) that don't produce XRD peaks that could rise significantly above background noise. Therefore, contributing only to noise in the XRD [51, 65, 66].

The peak broadening of NiO was attributed to lower crystallinity due to increased nickel vacancy creation/lattice active oxygen [67]. The lowering of  $2\theta$  values in the XRD pattern and a 2.5% increase in lattice parameter were observed [51]. The XRD analysis of peak broadening, the  $2\theta$  shift to lower angles, increase in lattice parameter, and lattice strain confirmed the presence of lattice active oxygen in raw NiO. XRD also gives evidence of the surface active oxygen presence due to the ample noise present in XRD. These facts together confirm the presence of active oxygen. A detailed analysis has been provided in an earlier publication [51]. The conventional iodometric investigation was repeated thrice to double-check the active oxygen, which was determined from the difference between total oxygen and stoichiometric oxygen [64, 68–70]. The active oxygen in NiO was estimated to be 10.47 wt%. The O/Ni ratio is found to be  $1.718 \pm 0.077$ , implying that sufficient non-stoichiometry exists in the NiO sample under study due to active oxygen [51]. To double-check the distribution of the named 'active oxygen' in lattice active oxygen and surface active oxygen, XPS was carried out.

### X-ray Photoelectron Spectroscopy

Figure 5 depicts the O(1 s) spectrum of the raw NiO. As evident from Fig. 5, NiO has two peaks at 529.6 eV and 531.6 eV binding energies. The binding energy of the first peak corresponds to the O (1 s) core level of  $O^{2-}$  anions involved in the chemical bonding of NiO [71–73]. The binding energy of the second peak corresponds to the oxygen atoms adjacent to the Ni vacancies within the NiO crystal structure. Several researchers have attributed the second peak to the oxygen defects [72–77]. In XPS, the percentage atomic concentration of

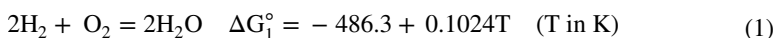
**Fig. 5** XPS spectra from O(1 s) core level of NiO

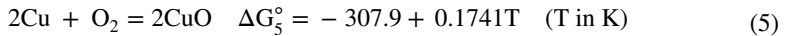
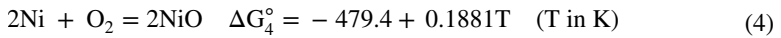
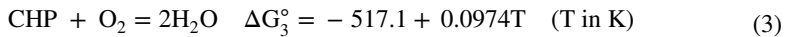


an element is estimated from the ratio of the peak area of that element to the overall area after background correction. When calculating the percentage atomic concentration, the respective peak areas are divided by their relative sensitivity factors (RSF). In the present case, both peaks correspond to the same element. Therefore, RSF being the same, the percentages of oxygen bonded to regular NiO crystal and defective oxygen have been calculated from the ratio of their respective areas to the total area. After subtracting the baseline from Fig. 5, the estimated areas of peak 1 [bonded O(1 s)] and peak 2 [defective O(1 s)] are 6540 and 7357, respectively; the atomic percentages of bonded O(1 s) and defective O(1 s), respectively, are 47 and 53 percent. This means that out of the total oxygen present in NiO, 47% are bonded to Ni, with the other 53% being defective. This gives rise to an O/Ni ratio of 2.127. This O/Ni ratio is higher than the O/Ni ratio estimated from iodometry (i.e., 1.718) [51]. Taking the average of these two, the estimated value of the O/Ni ratio is 1.922. The average O/Ni ratio has been estimated because XPS estimates only the O/Ni ratio of the surface with great accuracy and precision, whereas, iodometry determines the O/Ni ratio of the entire sample by volumetric chemical analysis by titration. Although iodometry determines the O/Ni ratio of the complete sample, which includes both surface and bulk oxygen, the precision and accuracy are likely to be lower than XPS, due to human errors. Therefore, the average ratio has been taken for thermodynamic calculations, as described later. The O/Ni ratio  $> 1$  has also been reported by several researchers [64, 67, 69, 71, 78–82]. It is widely accepted that NiO is a p-type oxide with a strong proclivity for the production of Ni vacancies as charge carriers and extra oxygen interstitial atoms, resulting in a non-stoichiometric  $\text{Ni}_{1-x}\text{O}$  crystal with the O/Ni ratio  $> 1$ . Karsthoof et al. [83] annealed NiO in the air at 973, 1373, and 1723 K, followed by heating in the vacuum at 293 to 773 K. After the evacuation at 298 K, the O/Ni ratio was estimated to be 2.5. Even after evacuating at 773 K, they couldn't eliminate the active oxygen. Dubey et al. [71] prepared NiO by thermal decomposition of  $\text{Ni}(\text{NO}_3)_2 \cdot 6\text{H}_2\text{O}$  at a temperature below 973 K. For the sample prepared at 673 K, the active oxygen was 39.51%, giving rise to O/Ni ratio  $> 1$ . Hala et al. [84] used DC reactive magnetron sputtering to make a thin layer of NiO, whose O/Ni ratio was found to be in the range of 1.40 to 1.41 as a function of discharge oxygen content. Non-stoichiometric NiO was synthesized and thermogravimetrically analyzed by Dubey et al. [78]. They concluded that the stoichiometry of NiO changes with sintering temperature, and the active oxygen decreases with an increase in the sintering temperature. However, even sintering NiO samples at 1373 K couldn't remove the active oxygen [63], indicating that NiO always contains active oxygen.

### Effect of Active Oxygen on Thermodynamics

Thermodynamics and kinetics are the potential pathways for the reduction of NiO, just as they are for all chemical processes. Thermodynamic feasibility is determined by the Gibbs standard free energy, denoted by  $\Delta G$ . The current study has been performed by CHP consisting of  $\text{H}_2$ , along with various excited species such as ro-vibrationally excited hydrogen molecules ( $\text{H}_2^*$ ), atomic hydrogen (H), etc. The  $\Delta G^\circ$  values of these plasma species and reactions of interest are represented below. The  $\Delta G^\circ$  of  $\text{CuO} \rightarrow \text{Cu}$  has been added for comparison.

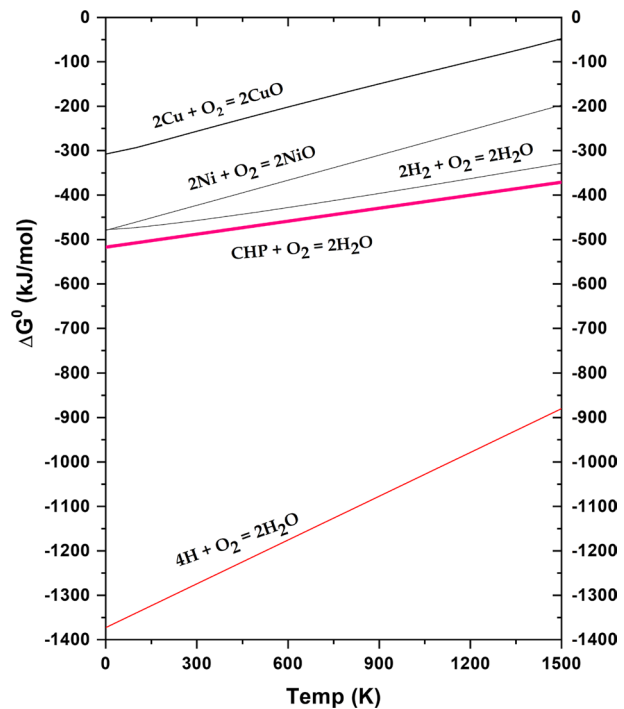




The Ellingham diagram for the above reactions is shown in Fig. 6.

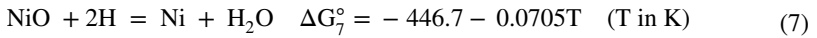
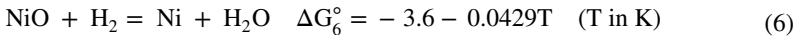
The Ellingham diagram's concept is that the metals laying below can reduce the top oxides. The greater is the difference in  $\Delta G^\circ$ , the more reduction is possible. As evident from Fig. 6, the  $\text{H}_2 \rightarrow \text{H}_2\text{O}$  line lies beneath the  $\text{Ni} \rightarrow \text{NiO}$  line, making the  $\Delta G^\circ$  difference almost negligible. This tiny difference of  $\Delta G^\circ$  does not make  $\text{H}_2$  a better reductant. However, the  $\Delta G^\circ$  of the  $\text{H} \rightarrow \text{H}_2\text{O}$  line is significantly lower. Apart from  $\text{H}$ , CHP also contains  $\text{H}_2^*$ , which lies between  $\text{H}_2$  and  $\text{H}$ , thus lowering the  $\Delta G^\circ$  value. These excited plasma species lower the  $\Delta G^\circ$  value, thereby increasing the  $\Delta G^\circ$  difference, confirming that CHP is a more potent reductant than  $\text{H}_2$ . This lowering of  $\Delta G^\circ$  due to CHP has also been reported earlier [57, 59, 61, 89]. However, the difference in  $\Delta G^\circ$  between  $\text{Ni} \rightarrow \text{NiO}$  and  $\text{CHP} \rightarrow \text{H}_2\text{O}$  is only around 38 kJ/mol. In contrast, the difference in  $\Delta G^\circ$  between  $\text{Cu} \rightarrow \text{CuO}$  and  $\text{CHP} \rightarrow \text{H}_2\text{O}$  is around 210 kJ/mol, making the reduction of  $\text{CuO}$  by CHP more feasible than  $\text{NiO}$ , as per the thermodynamic estimates from the Ellingham diagram. But the presence of active oxygen gives the opposite results, as explaining later.

**Fig. 6** Ellingham diagram for Cu–CuO, Ni–NiO,  $\text{H}_2$ – $\text{H}_2\text{O}$ , CHP– $\text{H}_2\text{O}$ , and  $\text{H}$ – $\text{H}_2\text{O}$  [61, 85–88]

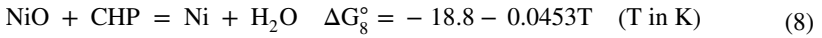




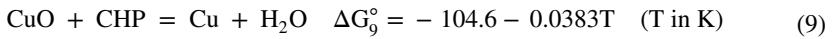
From the above Eqs. (1) – (5), the  $\Delta G^\circ$  of the reduction reactions for NiO with H<sub>2</sub>, H, and CHP, and reduction of CuO with CHP are framed, which are represented by the following reactions:



The reaction for CHP is



The reduction of CuO by CHP has been added for comparison, which is represented as:

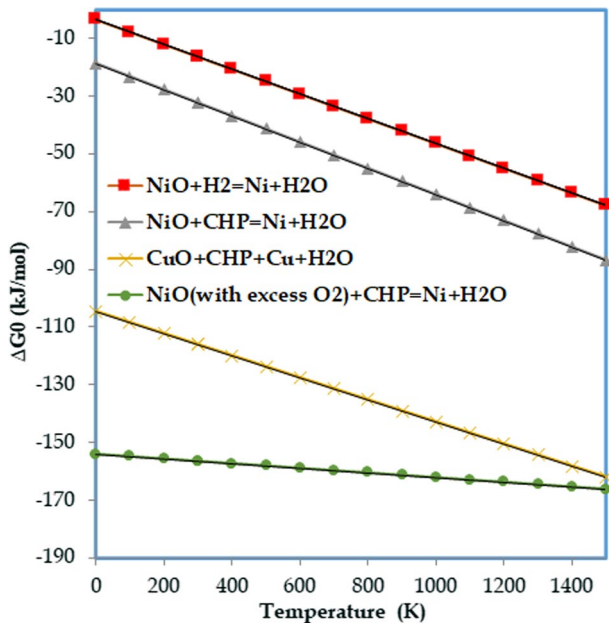


The  $\Delta G^\circ$  versus T of the above reactions are shown in Fig. 7.

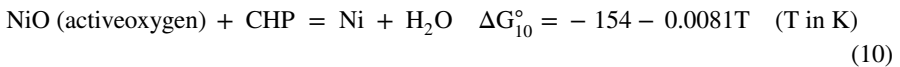
As evident from Fig. 7,  $\Delta G^\circ$  for the reduction of NiO by CHP (Eq. 8) is only around -18.8 kJ/mol at low temperature; therefore, CHP is not a potent reductant at low temperature. However,  $\Delta G^\circ$  for CuO → Cu is around -104.6 kJ/mol, which is significantly low compared to NiO → Ni. On the other hand, the presence of active oxygen in NiO, has been documented [51]. As a result, it's critical to examine if active oxygen has any effect on thermodynamics.

The influence of active oxygen on thermodynamics can be explained by the basic thermodynamic equation of reduction of NiO by CHP, which is given by Eq. 8. Equation 8 is composed of two half-reactions: (i) NiO = Ni + ½O<sub>2</sub> and (ii) CHP + ½O<sub>2</sub> = H<sub>2</sub>O, which are derived from the stoichiometric Eq. 4 and Eq. 3, respectively. Equation 4 is for a stoichiometric NiO with O/Ni ratio = 1; therefore, 1 mol of NiO produces 16 X

**Fig. 7** The  $\Delta G^\circ$  versus T plot of the reduction of NiO by H<sub>2</sub> and CHP, and CuO reduction by CHP [61, 85–88]



$10^{-3}$  kg of oxygen. This amount of oxygen is taken by CHP, giving rise to the estimated  $\Delta G^\circ$  value of Eq. 8. However, the O/Ni ratio of the NiO under current investigation is 1.922. This non-stoichiometric NiO produces higher oxygen (i.e.,  $25.68 \times 10^{-3}$  kg) than the  $16 \times 10^{-3}$  kg oxygen produced from the stoichiometric NiO from Eq. 4. As there is a continuous flow of  $H_2$  and there is no starvation of  $H_2$  species in CHP, this extra oxygen (12.96 wt%) is consumed by CHP (Eq. 3). Therefore, the  $\Delta G^\circ$  value of Eq. 3 changes accordingly. After incorporating the  $\Delta G^\circ$  of contribution from the active oxygen, the modified Eq. 8 can be written as:



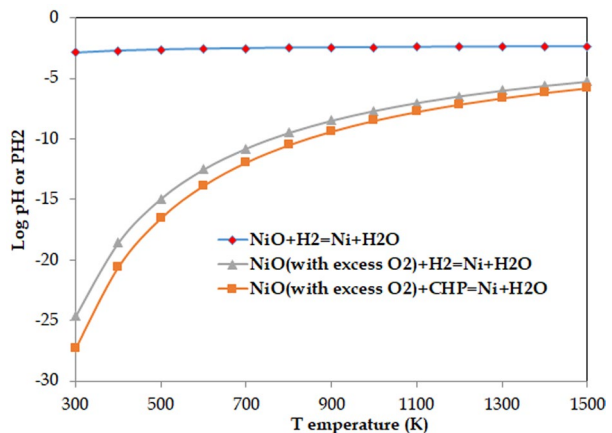
Comparing the  $\Delta G^\circ$  values Eq. 8 and Eq. 10, active oxygen addition decreases the  $G^\circ$  value by 135.2 kJ/mol. This decrease in  $\Delta G^\circ$  is so significant that it surpasses the significant  $\Delta G^\circ$  value of CuO reduction by CHP, as evident from Fig. 7. The significant decrease in  $\Delta G^\circ$  due to active oxygen can be explained in another way. The  $\Delta G^\circ$  used in Fig. 7 is a function of T and equilibrium constant ( $K$ ), mathematically expressed as  $\Delta G^\circ = -RT \ln K$ , where  $K = p_{H_2O}/p_{H_2}$ . With the increase in the active oxygen, there is an increase in the formation of  $H_2O$ , which leads to an increase in  $p_{H_2O}$ , thereby increasing the  $K$ , which makes  $\Delta G^\circ$  more negative. This could be the reason for easier and faster NiO~Ni reduction than CuO~Cu. NiO~Ni reduction takes only 300 s, whereas CuO~Cu takes 1200 s. An important inference comes from these results, that while using the CHP for the production of Ni from NiO, the active oxygen plays an important role.

Further, putting  $K = p_{H_2O}/p_{H_2}$  in the  $\Delta G^\circ$  expression and simplifying, the B-G equilibrium diagram was worked out [52, 54, 62], shown in Fig. 8.

Figure 8 shows the equilibrium partial pressure of  $H_2$  required for NiO  $\rightarrow$  Ni reduction at various temperatures. The B-G diagram provides very important inferences. Firstly, there is a decrease of equilibrium partial pressure of  $H_2$  required for NiO  $\rightarrow$  Ni reduction with a decrease in temperature. The decrease is only marginal. However, the drop is much sharper for active oxygen, favoring the reduction of NiO at lower temperatures.

Furthermore, in the presence of CHP, the decline becomes further sharper, thereby supporting the feasibility of reduction of active oxygen-containing NiO at low

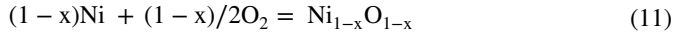
**Fig. 8** Bauer–Glaessner diagram of variation in hydrogen partial pressure with temperature [61, 85–88]



temperature by CHP. Therefore, both active oxygen and CHP support the reduction at low temperatures. As NiO always contains active oxygen, the NiO → Ni reduction process by CHP becomes important for industrial application.

However, the heart of the matter in the current investigation, are the changes in the enthalpy of formation and entropy due to the non-stoichiometry of the Ni<sub>1-x</sub>O. As a result, estimations of the dependency of the enthalpy of formation and entropy on x in Ni<sub>1-x</sub>O are critical, therefore, evaluated here.

Equation (4) can be written as:



The ΔG for this reaction is:

$$\Delta G_{11}^\circ = (1 - x)(-239.7) + (1 - x)0.0940T \quad (T \text{ in K}) \tag{12}$$

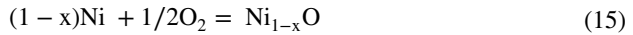
The reaction for active oxygen can be expressed as:



The ΔG for Eq. (13) can be estimated [85] by:

$$\Delta G_{13}^\circ = x(251.6 - 0.652T) \tag{14}$$

When Eqs. (11) and (13) are combined, the equation for formation of Ni<sub>1-x</sub>O is written as:



ΔG for this reaction can be obtained by combining ΔG° of Eqs. (12) and (14):

$$\Delta G_{15}^\circ = (-239.7 + 491.3x) - (-0.940 + 0.1592x)T \tag{16}$$

From Eq. (16), the dependance of enthalpy of formation (ΔH<sub>f</sub>) and ΔS, on x of Ni<sub>1-x</sub>O has been estimated, which as shown in Fig. 9.

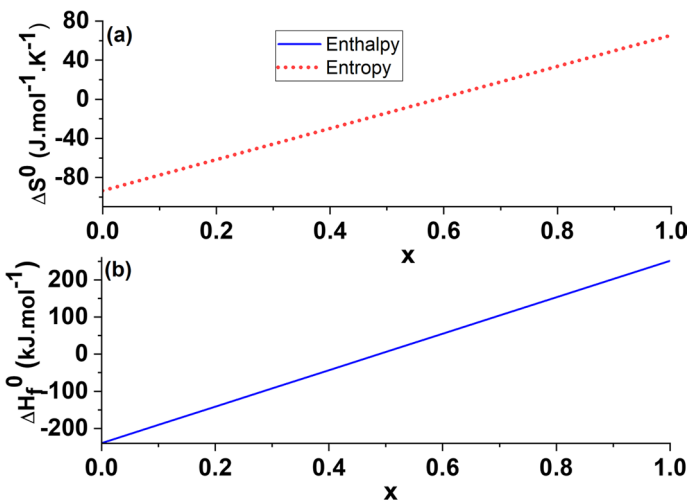


Fig. 9 Dependence of enthalpy of formation (ΔH<sub>f</sub>) and entropy (ΔS) on x in Ni<sub>1-x</sub>O

As clearly evident from Fig. 9, both  $\Delta H_f$  and  $\Delta S$  increase with increase in  $x$ , thermodynamically decreasing the stability of  $Ni_{1-x}O$ . Once the Ni–O bond stability decreases, less energy required to break the bond, making the reduction easier.

As described above, the Ellingham Diagram (Fig. 6),  $\Delta G^\circ$  versus  $T$  diagram of the reduction reactions (Fig. 7), and B-G Diagram (Fig. 8) show that the presence of active oxygen substantially promotes the reduction of NiO by CHP. This is further supported by the fact that active oxygen reduces the bond stability of  $Ni_{1-x}O$ , making reduction easier.

## Effect of Active Oxygen on the Kinetics

According to the above thermodynamic analysis, the presence of active oxygen strongly favors the reduction of  $NiO \rightarrow Ni$  by  $H_2$  or CHP. Furthermore, when the non-stoichiometry afforded by active oxygen increases, the thermodynamic stability of  $Ni_{1-x}O$  declines. Both these findings motivated the investigation of the kinetics of  $Ni_{1-x}O$  reduction. The kinetics studies of stoichiometric oxides by CHP using the same experimental setup, have already been reported [53, 54, 57–59, 62]. In all these earlier studies, the reaction was interrupted and the samples weighed, and various models could be successfully fitted to the experimental data. For example, Johnson and Mehl, Avrami, and Erofeev equation [58, 59, 62], moving-interface [54], Arrhenius equation [53], and other rate equations. In these kinetic investigations, the percentage reduction (i.e., degree of conversion), was calculated using the same manner as previously described. The same methodology has also been used in the current investigation of non-stoichiometric  $Ni_{1-x}O$ . However, in case of  $Ni_{1-x}O$ , the percentage reduction exceeded 100%, as shown in Table 1. Several attempts were made to overcome this issue by utilizing the results of divergence from stoichiometry, as obtained from iodometry and XPS investigations. Various rate equations were explored, but none of them could fit the experimental data. This is because active oxygen levels are not uniform throughout the sample, as evidenced by XPS and instant pressure increase at the beginning of reduction. XPS results showed 100% active oxygen at the surface [47% bonded O(1 s) and 53% defective O(1 s)], whereas only 47% of active oxygen [i.e., lattice active oxygen or bonded O(1 s)] remains at the bulk. Therefore, the active oxygen available at the surface is higher than the active oxygen at the bulk. This was also observed by Deren and Stoch [64], after a thorough analysis of the results of the earlier researchers. They also reported that NiO is always associated with surface active oxygen due to the chemisorption of oxygen at the surface, which can be easily removed compared to lattice active oxygen. This is the reason of the increase in pressure at the beginning of reduction, as illustrated in Fig. 10. This increase in pressure is due to the evolution of  $H_2O$  vapor carrying the exothermic reaction heat produced (Eq. 3) when the CHP reacts rapidly with the weakly bound active oxygen at the surface. The surface active oxygen could also be the reason that none of the earlier researchers could report the role of active oxygen in kinetic analysis of the reduction of NiO by  $H_2$  or CHP.

However, active oxygen in NiO has been shown to affect the activation energy of carbon monoxide oxidation over multiple nickel oxide catalysts in varied conditions [90]. Nevertheless, Richardson et al. [91] discussed that their prepared NiO crystallites contained active oxygen, which was removed from the sample by passing the reducing gas  $H_2$  over it. The removal of active oxygen created vacancies. The same thing was noticed by Rodriguez et al. [35] and Kim et al. [67], during the induction period. However, none of the researchers looked into the influence of active oxygen on the kinetics of the reduction of

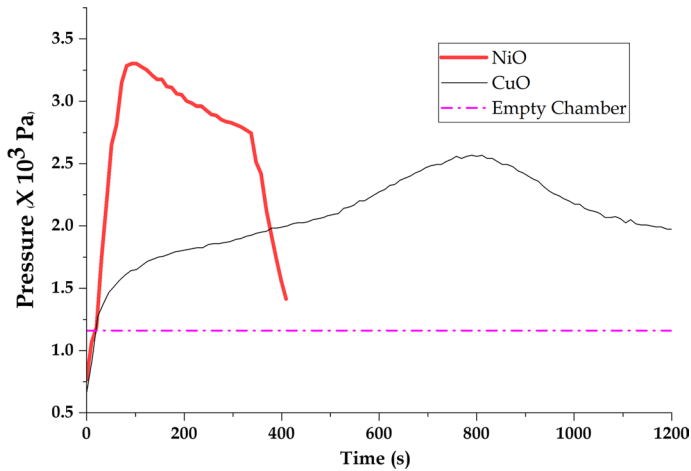


**Fig. 10** Variation of pressure for CuO and NiO at hydrogen flow rate  $2.5 \times 10^{-6} \text{ m}^3 \text{ s}^{-1}$  and 750 W

NiO. Therefore, the current research attempted to investigate the role of active oxygen in the NiO  $\rightarrow$  Ni reduction kinetics.

It is important to mention here that CHP is nothing more than an excited state of  $\text{H}_2$  gas. The excitation is provided by an electromagnetic wave, in this case, a microwave. The NiO pellet is covered by the microwave CHP that forms locally. The reduction begins at the CHP-NiO interface, which resembles a gas–solid reaction in many ways. Therefore, it is reasonable to take the reduction kinetics of gas–solid reactions as a reference. The kinetics of reduction in gas–solid reactions are well-known and have been discussed elsewhere [92–96]. Sohn [96] addressed the elementary steps that provide the foundation for gas–solid reactions. The concepts of gas–solid reactions have been applied to the current investigation. The corresponding elementary steps in the CHP-NiO reduction are:

1. External mass transfer of  $\text{H}_2$  to form CHP at the CHP-pellet interface,
2. Mass transfer of CHP species through the Ni product layer to the CHP-NiO reduction interface,
3. Reduction reaction at the CHP-NiO interface (including the absorption of CHP species and desorption of water vapor),
4. Outward diffusion of the reduction product  $\text{H}_2\text{O}$  vapor from the Ni-NiO interface to CHP-Ni interface,
5. Diffusion of the product  $\text{H}_2\text{O}$  vapor from the CHP-pellet interface to the bulk.

These kinetic steps could be successfully applied for the application of rate laws in the earlier investigations [53, 54, 57–59, 62]. Furthermore, the difficulty in applying rate laws in the current investigation is due to active oxygen, which gives rise to the problem of higher reduction than actual [51], making the estimated percentage reduction also exceeds 100%, therefore, making the application of rate laws problematic. NiO  $\rightarrow$  Ni reduction is also linked to a number of other difficulties, including the induction period, wide variation of activation energies, and a lack of concordance with any kinetic model, as mentioned earlier. One of the key causes of the problems mentioned above could be the active oxygen, which has not been reported yet. To evaluate the effect of active

oxygen, a comparison with a stoichiometric oxide is necessary, with all reduction kinetic parameters being kept virtually similar. CuO is selected because the reduction of NiO is quite comparable to CuO. Both showed delayed reduction due to the incubation period, followed by auto-catalytic reduction [35, 36, 43, 38, 62, 97, 98]. However, CuO is stoichiometric and thermodynamically less stable than NiO (as shown in Fig. 6). As a result, if CuO and NiO are reduced using the same kinetics parameters, CuO should be easier to reduce than NiO. Therefore, a comparative study has been carried out, to examine whether there is any effect of active oxygen on kinetics.

The kinetic steps outlined above were attempted to be applied to the reduction studies of CuO and NiO. Concerning the kinetic steps, the external mass transfer (kinetic step 1) is the same for both CuO and NiO because both were reduced at  $2.500 \times 10^{-6} \text{ m}^3 \text{ s}^{-1} \text{ H}_2$  flowrate and microwave power of 750 W. The kinetic step 5 is controlled by pumping out the gas out of the chamber. When reduction processes are not taking place inside the reduction chamber, the microwave-assisted plasma reactor employed for this study is designed so that only a specific set pressure is reached inside the experimental chamber for a particular flow rate. Therefore, kinetic step-5 is same for NiO and CuO. This is accomplished by pumping the gas out of the empty chamber to maintain constant pressure. This has been shown as the dotted line in Fig. 10. However, when a reduction reaction takes place,  $\text{H}_2\text{O}$  vapor is produced as a reaction product. Due to the reduction, one activated  $\text{H}_2$  molecule is replaced by one  $\text{H}_2\text{O}$  molecule, with no increase in the overall gaseous species present. However, the pressure increases due to the reduction heat (Eq. 3) produced at the reduction interface. The increase of pressure generated by the heating of the produced  $\text{H}_2\text{O}$  vapor adds up to the specified value of the attained pressure for that particular flow rate, thereby increasing the chamber pressure. The increase in chamber pressure for NiO and CuO is shown in Fig. 10. This pressure rise has also been observed during reductions of other metal oxides and their mixtures [53, 54, 57–59, 62]. The elementary steps 2 and 4 have been taken care of by making the surface flat and making the pellet thickness small and the diameter to thickness ratio large. Steps 2 and 4 (inward and outward diffusion) are also corroborated by a similar decrease of molar volume, i.e., 41% decrease in molar volume during  $\text{NiO} \rightarrow \text{Ni}$  reduction and 43% decrease in molar volume during  $\text{CuO} \rightarrow \text{Cu}$  reduction [62].

However, CuO is stoichiometric and doesn't contain surface oxygen. In contrast, surface active oxygen is always present in NiO [64]. Deren and Stoch [64] reported that NiO is always associated with surface active oxygen due to the chemisorption of oxygen at the surface, which can be easily removed compared to lattice active oxygen. In the current investigation, the O/Ni ratio = 1.922, therefore, likely to enhance the diffusion by removing the extra oxygen and creating more rooms for diffusion. Unlike CuO, the removal of surface active oxygen in NiO would create the diffusion paths for plasma species, increasing the diffusion of plasma species to the reduction interface.

Step 3 has been controlled for both CuO and NiO pellets by maintaining the same plasma parameters (microwave power of 750 W and  $\text{H}_2$  flow rate of  $2.500 \times 10^{-6} \text{ m}^3 \text{ s}^{-1}$ ) throughout the experiments [53, 54, 57–59, 62]. The comparison of kinetic steps are provided in Table 2.

As discussed, and summarized in Table 2, active oxygen gives porosity, increasing the inward diffusion of CHP species (i.e., step-2) and outward diffusion of reaction product  $\text{H}_2\text{O}$  vapor (i.e., step-4). It also enhances the thermodynamic feasibility (i.e., step-3) by lowering the  $\Delta G$  and producing more reaction heat. Also, as the quantity of surface active oxygen is high and they are loosely bound, the removal of surface active oxygen is easier. All these factors contribute to the enhancement of  $\text{NiO} \rightarrow \text{Ni}$  reduction. This results in more reaction

**Table 2** Comparison of kinetic steps of CuO and NiO

Elementary steps	CuO	NiO
Step-1	Same	Same
Step-2	Porosity and morphology are nearly the same. The molar volume change is 43%	Porosity and morphology are nearly the same. The molar volume change is 41%. Removal of active oxygen creates more porosity, thereby making the inward diffusion of plasma species to the reduction interface easier. Therefore, kinetically more favorable
Step-3	Equation 9: $\text{CuO} + \text{CHP} = \text{Cu} + \text{H}_2\text{O}$ ; $\Delta G_9 = -104.6 - 0.0383 \text{ T}$	Equation 10: $\text{NiO} (\text{active oxygen}) + \text{CHP} = \text{Ni} + \text{H}_2\text{O}$ ; $\Delta G_{10} = -154 + 0.0081 \text{ T}$ . Active oxygen significantly lowers the $\Delta G$ , making $\text{NiO} \rightarrow \text{Ni}$ more thermodynamically feasible. Furthermore, more reaction heat ( $\Delta H$ ) is produced
Step-4	The molar volume change is 43%	The molar volume change is 41%. Removal of active oxygen creates more porosity and produces more reaction heat, thereby making the outward diffusion of $\text{H}_2\text{O}$ vapor easier. Hence, kinetically more favorable
Step-5	Same	Same

heat, which heats the reduction product  $\text{H}_2\text{O}$  vapor, thereby increasing the chamber pressure. A detailed comparison of the pressure has been made in Fig. 10.

It is well known that the gas–solid reaction starts at the interface. The gas absorption at the interface is considered one of the elementary rate-controlling steps in gas–solid reactions [92, 95, 96, 99]. In the current investigation, CHP first interacts with the top surface of the NiO pellet at the CHP–NiO interface. If surface active oxygen is available at the surface and absorption of excited species in the CHP–NiO interface is not rate-controlling, the reduction should start immediately. If the reduction of CHP–NiO starts immediately, then the hot reduction product  $\text{H}_2\text{O}$  vapor would be produced, leading to increased pressure. As mentioned earlier, only a particular pressure is attained inside the experimental chamber for a particular flow rate in the empty chamber. But when some reduction reaction is taking place, there is the evolution of reaction heat and product  $\text{H}_2\text{O}$  vapor. As explained earlier, this pressure due to the produced hot  $\text{H}_2\text{O}$  vapor adds up to the particular set value of the attained pressure for that particular flow rate, increasing the chamber pressure. This increase in pressure has already been reported during the reduction of other metal oxides and their mixtures [53, 54, 57–59, 62].

The chamber pressure for NiO and CuO are shown in Fig. 10.

As evident from Fig. 10, the chamber pressure for CuO increases slowly, whereas the pressure for NiO rises instantly. Time taken for attaining the maximum chamber pressure is around 100 s for NiO, whereas CuO takes approximately 800 s. The maximum chamber pressure for NiO is  $3.300 \times 10^3$  Pa, compared to  $2.475 \times 10^3$  Pa for CuO. NiO achieves more pressure in lesser time, indicating that NiO is reduced very fast compared to CuO, even though the reduction of  $\text{CuO} \rightarrow \text{Cu}$  by  $\text{H}_2$  is thermodynamically more feasible than the reduction of  $\text{NiO} \rightarrow \text{Ni}$ . The more apparent reduction of NiO is confirmed from the experimental results (Table 1). As shown in Table 1, CuO takes 1200 s for a complete reduction compared to 300 s for NiO. Such a vast difference in time for the complete reduction, faster reduction rate, and increased pressure have enormous practical implications..

The rise in pressure comes within a few seconds of the beginning of reduction due to the instant absorption of excited species at the CHP–NiO interface and reaction of CHP with the surface active oxygen, leading to the formation of  $\text{H}_2\text{O}$  vapor. The increase in pressure may be primarily due to surface active oxygen (Eq. 3) because the pressure rise is instant. However, the contribution of the lattice active oxygen can't be ruled out. Nevertheless, the instant evolution of hot water vapor, hence, faster reduction, is due to active oxygen.

The current investigation yielded an outstanding result; namely, active oxygen increases both the thermodynamic and kinetic potentials, thereby speeding up the reaction, which is helpful for NiO reduction. This fact is also important for other extraction processes, but it has not yet been highlighted. The use of CHP and active oxygen, both of which enhance diffusion, will greatly help diffusion-controlled extraction operations. Because CHP can reduce most of the metal oxides [53, 54, 57, 62] and oxide mixtures [57–59], and oxide ores primarily contain oxides; these recent findings of the massive enhancement of thermodynamics and kinetics of NiO reduction by active oxygen and CHP, will open up many new research avenues in the future, including strategically examining the effect of active oxygen in most oxide ores extraction processes, including oxide ores of Ni.



## Conclusions

The following conclusions can be taken from the current study of nickel oxide reduction by cold hydrogen plasma:

1. Active oxygen is present in nickel oxide, thereby making it non-stoichiometric.
2. Active oxygen consists of surface active oxygen and lattice active oxygen.
3. Active oxygen decreases the stability of NiO.
4. Active oxygen lowers the Gibbs standard free energy of NiO  $\rightarrow$  Ni reduction, thereby making reduction more feasible.
5. The presence of excited plasma species in CHP further decreases the Gibbs standard free energy of NiO  $\rightarrow$  Ni reduction. Thus, making CHP a more potent reductant for the reduction of NiO containing active oxygen.
6. The equilibrium partial pressure of molecular hydrogen required for NiO  $\rightarrow$  Ni reduction decreases only marginally with decreasing temperature. The active oxygen decreases the equilibrium partial pressure significantly with decreasing temperature. CHP reduces it further, confirming the feasibility of CHP reduction of NiO  $\rightarrow$  Ni reduction at low temperatures.
7. The presence of active oxygen increases the porosity, thereby supporting the diffusion. The reduction starts instantly, and the reduction becomes faster.
8. These factors help speed up reduction to the point that a  $7.5 \times 10^{-6}$  kg pellet can be reduced in 1200 s utilizing 600 W microwave power and a hydrogen flow rate of  $1.166 \times 10^{-6}$  m<sup>3</sup> s<sup>-1</sup>, thus opening up the up scalability for NiO reduction by CHP.
9. As CHP can reduce most of the metal oxides, and the oxide ores mainly contain oxides, this current finding of the enormous enhancement of reduction by active oxygen would explore many research areas in the future, strategically examining the effect of the presence of active oxygen in most of the metal extraction processes from oxide ores, especially, oxide ores of Nickel,

**Acknowledgements** I am thankful to Prof. (Dr.) Barada Kanta Mishra, Director, Indian Institute of Technology Goa, India, and Prof. (Dr.) Raja Kishore Paramguru, Professor (Retd.), Mechanical Engineering, KIIT and Chief Scientist (Retd.) CSIR-IMMT, Bhubaneswar, India, for their guidance throughout my research. I would also like to thank CSIR, New Delhi, for providing financial support to carry out research work under the project MINMET, Project No. ESC 205.

## References

1. Oxley A, Smith ME, Caceres O (2016) Why heap leach nickel laterites? *Miner Eng* 88:53–60. <https://doi.org/10.1016/j.mineng.2015.09.018>
2. Petrus HTBM, Putera ADP, Sugiarto E et al (2019) Kinetics on roasting reduction of limonitic laterite ore using coconut-charcoal and anthracite reductants. *Miner Eng* 132:126–133. <https://doi.org/10.1016/j.mineng.2018.11.043>
3. Oliveira C, Freitas FM, Abreu GJP et al (2014) Optical measurements of atmospheric pressure direct current He/H<sub>2</sub> microplasma in open air for surface modification. *Am J Condens Matter Phys* 4:19–27. <https://doi.org/10.5923/s.ajcmp.201401.03>
4. Zhu D, Pan L, Guo Z et al (2019) Utilization of limonitic nickel laterite to produce ferronickel concentrate by the selective reduction-magnetic separation process. *Adv Powder Technol* 30:451–460. <https://doi.org/10.1016/j.apt.2018.11.024>

5. Ma B, Wang C, Yang W et al (2013) Screening and reduction roasting of limonitic laterite and ammonia-carbonate leaching of nickel-cobalt to produce a high-grade iron concentrate. *Miner Eng* 50–51:106–113. <https://doi.org/10.1016/j.mineng.2013.06.014>
6. Garcés-Granda A, Lapidus GT, Restrepo-Baena OJ (2018) The effect of calcination as pre treatment to enhance the nickel extraction from low-grade laterites. *Miner Eng* 120:127–131. <https://doi.org/10.1016/j.mineng.2018.02.019>
7. Kaya S, Topkaya YA (2011) High pressure acid leaching of a refractory lateritic nickel ore. *Miner Eng* 24:1188–1197. <https://doi.org/10.1016/j.mineng.2011.05.004>
8. Pickles CA, Anthony W (2018) Thermodynamic modelling of the reduction of a saprolitic laterite ore by methane. *Miner Eng* 120:47–59. <https://doi.org/10.1016/j.mineng.2018.02.006>
9. Meshram P, Abhilash PBD (2019) Advanced review on extraction of nickel from primary and secondary sources. *Miner Process Extr Metall Rev* 40:157–193. <https://doi.org/10.1080/08827508.2018.1514300>
10. Rodrigues F, Pickles CA, Peacey J et al (2017) Factors affecting the upgrading of a nickeliferous limonitic laterite ore by reduction roasting, thermal growth and magnetic separation. *Minerals* 7:176. <https://doi.org/10.3390/min7090176>
11. Moats MS, Davenport WG (2014) Nickel and cobalt production. *Treatise on process metallurgy*, vol 3. Elsevier, Amsterdam, pp 625–669
12. Burkin AR (1987) *Extractive metallurgy of nickel*. Wiley, New York
13. Elliott R, Pickles CA, Peacey J (2017) Ferronickel particle formation during the carbothermic reduction of a limonitic laterite ore. *Miner Eng* 100:166–176. <https://doi.org/10.1016/j.mineng.2016.10.020>
14. Pickles CA, Forster J, Elliott R (2014) Thermodynamic analysis of the carbothermic reduction roasting of a nickeliferous limonitic laterite ore. *Miner Eng* 65:33–40. <https://doi.org/10.1016/j.mineng.2014.05.006>
15. Yang J, Zhang G, Ostrovski O, Jahanshahi S (2019) Selective reduction of an Australian garnieritic laterite ore. *Miner Eng* 131:79–89. <https://doi.org/10.1016/j.mineng.2018.10.018>
16. Rao M, Li G, Jiang T et al (2013) Carbothermic reduction of nickeliferous laterite ores for nickel pig iron production in China: a review. *JOM* 65:1573–1583. <https://doi.org/10.1007/s11837-013-0760-7>
17. Sridhar S, Sichen DU, Seetharaman S (1994) Investigation of the kinetics of reduction of nickel oxide and nickel aluminate by hydrogen. *Zeitschrift fuer Met* 85:616–620
18. de Alvarenga OV, dos Santos CG, de Albuquerque BE (2019) Assessing the influence of NaCl on the reduction of a siliceous laterite nickel ore under caron process conditions. *Metall Mater Trans B Process Metall Mater Process Sci* 50(3):1309–1321. <https://doi.org/10.1007/s11663-019-01552-w>
19. Visweswaran S, Venkatachalapathy R, Haris M, Murugesan R (2020) Structural, morphological, optical and magnetic properties of sprayed NiO thin films by perfume atomizer. *Appl Phys A Mater Sci Process* 126:1–12. <https://doi.org/10.1007/s00339-020-03709-w>
20. Gomaa MM, Yazdi GR, Schmidt S et al (2017) Effect of precursor solutions on the structural and optical properties of sprayed NiO thin films. *Mater Sci Semicond Process* 64:32–38. <https://doi.org/10.1016/j.mssp.2017.03.009>
21. Fedorov AV, Kukushkin RG, Yeletsky PM et al (2020) Temperature-programmed reduction of model CuO, NiO and mixed CuO–NiO catalysts with hydrogen. *J Alloys Compd* 844:156135. <https://doi.org/10.1016/j.jallcom.2020.156135>
22. Imran Din M, Rani A (2016) Recent advances in the synthesis and stabilization of nickel and nickel oxide nanoparticles: a green adeptness. *Int J Anal Chem*. <https://doi.org/10.1155/2016/3512145>
23. Ma B, Xing P, Yang W et al (2017) Solid-state metalized reduction of magnesium-rich low-nickel oxide ores using coal as the reductant based on thermodynamic analysis. *Metall Mater Trans B* 48:2037–2046. <https://doi.org/10.1007/s11663-017-0977>
24. Kharchenko YV, Blikharsky ZY, Vira VV, Vasylyv BD (2019) Study of structural changes in a nickel oxide containing anode material during reduction and oxidation at 600°C. In: Fesenko O, Yatsenko L (eds) *Nanocomposites, nanostructures, and their applications*. NANO 2018. Springer Proceedings in Physics, vol 221. Springer, Cham. [https://doi.org/10.1007/978-3-030-17759-1\\_42](https://doi.org/10.1007/978-3-030-17759-1_42)
25. Bakhshandeha SS, Setoudeh N, Ali Askari Zamanic M et al (2019) Carbothermic reduction of nickel oxide. *Adv Process Mater Eng* 13:63–75
26. Quiroz Cabascango VE, Yu Bazhin V, Cabascango VEQ, Bazhin VY (2020) Nickel oxide reduction in CO/CO<sub>2</sub> gas mixtures in reverberatory furnaces. *J Phys Conf Ser* 1515:22028. <https://doi.org/10.1088/1742-6596/1515/2/022028>
27. Che Abdullah SS, Mohd Nasri NN, Ahmad Zaidi NH et al (2020) Effect of H<sub>2</sub>/N<sub>2</sub> mixtures on reduction of nickel oxide. *Materials Science Forum*. Trans Tech Publ, Switzerland, pp 280–285

28. Ahmad F, Lovell EC, Masood H et al (2020) Low-temperature CO<sub>2</sub> methanation: synergistic effects in plasma-Ni hybrid catalytic system. *ACS Sustain Chem Eng* 8:1888–1898. <https://doi.org/10.1021/acssuschemeng.9b06180>
29. Kharatyan SL, Chatilyan HA, Manukyan KV (2019) Kinetics and mechanism of nickel oxide reduction by methane. *J Phys Chem C* 123:21513–21521. <https://doi.org/10.1021/acs.jpcc.9b04506>
30. Hidayat T, Rhamdhani MA, Jak E, Hayes PC (2009) Investigation of nickel product structures developed during the gaseous reduction of solid nickel oxide. *Metall Mater Trans B Process Metall Mater Process Sci* 40:462–473. <https://doi.org/10.1007/s11663-009-9247-x>
31. Hidayat T, Rhamdhani MA, Jak E, Hayes PC (2009) The kinetics of reduction of dense synthetic nickel oxide in H<sub>2</sub>-N<sub>2</sub> and H<sub>2</sub>-H<sub>2</sub>O atmospheres. *Metall Mater Trans B Process Metall Mater Process Sci* 40:1–16. <https://doi.org/10.1007/s11663-008-9212-0>
32. Hidayat T, Rhamdhani MA, Jak E, Hayes PC (2009) On the relationships between the kinetics and mechanisms of gaseous hydrogen reduction of solid nickel oxide. *Metall Mater Trans B Process Metall Mater Process Sci* 40:474–489. <https://doi.org/10.1007/s11663-009-9239-x>
33. Hidayat T, Rhamdhani MA, Jak E, Hayes PC (2008) The characterization of nickel metal pore structures and the measurement of intrinsic reaction rate during the reduction of nickel oxide in H<sub>2</sub>-N<sub>2</sub> and H<sub>2</sub>-H<sub>2</sub>O atmospheres. *Miner Eng* 21:157–166. <https://doi.org/10.1016/j.mineng.2007.09.004>
34. Benton AF, Emmett PH (1924) The reduction of nickelous and ferric oxides by hydrogen. *J Am Chem Soc* 46:2728–2737. <https://doi.org/10.1021/ja01677a018>
35. Rodriguez JA, Hanson JC, Frenkel AI et al (2002) Experimental and theoretical studies on the reaction of H<sub>2</sub> with NiO: role of O vacancies and mechanism for oxide reduction. *J Am Chem Soc* 124:346–354. <https://doi.org/10.1021/ja0121080>
36. Richardson JJT, Scates RMR, Twigg MVM (2004) X-Ray diffraction study of the hydrogen reduction of NiO/ $\alpha$ -Al<sub>2</sub>O<sub>3</sub> steam reforming catalysts. *Appl Catal A Gen* 267:35–46. <https://doi.org/10.1016/j.apcata.2004.02.022>
37. Jeangros Q, Hansen TW, Wagner JB et al (2013) Reduction of nickel oxide particles by hydrogen studied in an environmental TEM. *J Mater Sci* 48:2893–2907. <https://doi.org/10.1007/s10853-012-7001-2>
38. Manukyan KV, Avetisyan AG, Shuck CE et al (2015) Nickel oxide reduction by hydrogen: kinetics and structural transformations. *J Phys Chem C* 119:16131–16138. <https://doi.org/10.1021/acs.jpcc.5b04313>
39. Lee DS, Min DJ (2019) A kinetics of hydrogen reduction of nickel oxide at moderate temperature. *Met Mater Int* 25:982–990. <https://doi.org/10.1007/s12540-019-00261-y>
40. Yu D, Zhu M, Utigard TA, Barati M (2013) TGA kinetic study on the hydrogen reduction of an iron nickel oxide. *Miner Eng* 54:32–38. <https://doi.org/10.1016/j.mineng.2013.03.018>
41. Chatterjee R, Banerjee SSS, Banerjee SSS, Ghosh D (2012) Reduction of nickel oxide powder and pellet by hydrogen. *Trans Indian Inst Met* 65:265–273. <https://doi.org/10.1007/s12666-012-0130-0>
42. L'vov BV, Galwey AK, L'vov BV et al (2012) The mechanism and kinetics of NiO reduction by hydrogen Thermochemical approach. *J Therm Anal Calorim* 110:601–610. <https://doi.org/10.1007/s10973-011-2000-0>
43. Richardson JT, Scates R, Twigg MV (2003) X-ray diffraction study of nickel oxide reduction by hydrogen. *Appl Catal A Gen* 246:137–150. [https://doi.org/10.1016/S0926-860X\(02\)00669-5](https://doi.org/10.1016/S0926-860X(02)00669-5)
44. Zhou Z, Han L, Bollas GM (2014) Kinetics of NiO reduction by H<sub>2</sub> and Ni oxidation at conditions relevant to chemical-looping combustion and reforming. *Int J Hydrogen Energy* 39:8535–8556. <https://doi.org/10.1016/j.ijhydene.2014.03.161>
45. Avrami M (1940) Kinetics of phase change. II Transformation-time relations for random distribution of nuclei. *J Chem Phys* 8:212–224. <https://doi.org/10.1063/1.1750631>
46. Avrami M (1939) Kinetics of phase change. I: general theory. *J Chem Phys* 7:1103–1112. <https://doi.org/10.1063/1.1750380>
47. Chen F, Mohassab Y, Zhang S, Sohn HY (2015) Kinetics of the reduction of hematite concentrate particles by carbon monoxide relevant to a novel flash ironmaking process. *Metall Mater Trans B Process Metall Mater Process Sci* 46:1716–1728. <https://doi.org/10.1007/s11663-015-0345-7>
48. Szekely J, Lin CII, Sohn HYY (1973) A structural model for gas-solid reactions with a moving boundary-V an experimental study of the reduction of porous nickel-oxide pellets with hydrogen. *Chem Eng Sci* 28:1975–1989. [https://doi.org/10.1016/0009-2509\(73\)85042-0](https://doi.org/10.1016/0009-2509(73)85042-0)
49. Szekely J, Evans JWW (1971) A structural model for gas-solid reactions with a moving boundary-II. *Chem Eng Sci* 26:1901–1913. [https://doi.org/10.1016/0009-2509\(71\)86033-5](https://doi.org/10.1016/0009-2509(71)86033-5)
50. Adnadević B, Janković B (2008) Dispersive kinetic model for the non-isothermal reduction of nickel oxide by hydrogen. *Phys B Condens Matter* 403:4132–4138. <https://doi.org/10.1016/j.physb.2008.08.020>

51. Sabat KC (2021) Production of nickel by cold hydrogen plasma. *Plasma Chem Plasma Process* 41:1329–1345. <https://doi.org/10.1007/s11090-021-10194-3>
52. Sabat KC, Rajput P, Paramguru RK et al (2014) Reduction of oxide minerals by hydrogen plasma: an overview. *Plasma Chem Plasma Process* 34:1–23. <https://doi.org/10.1007/s11090-013-9484-2>
53. Rajput P, Sabat KC, Paramguru RK et al (2014) Direct reduction of iron in low temperature hydrogen plasma. *Ironmak Steelmak* 41:721–731. <https://doi.org/10.1179/1743281214Y.0000000186>
54. Sabat KC, Paramguru RK, Pradhan S, Mishra BK (2015) Reduction of cobalt oxide (Co<sub>3</sub>O<sub>4</sub>) by low temperature hydrogen plasma. *Plasma Chem Plasma Process* 35:387–399. <https://doi.org/10.1007/s11090-014-9602-9>
55. Sabat KC (2019) Hydrogen Plasma - Thermodynamics. In: *Journal of Physics: Conference Series*. Institute of Physics Publishing, pp 1–20. <https://doi.org/10.1088/1742-6596/1172/1/012086>
56. Sabat KC (2019) Iron production by hydrogen plasma. In: *International Conference on Applied Physics, Power and Material Science*. Institute of Physics Publishing, pp 1–5. <https://doi.org/10.1088/1742-6596/1172/1/012043>
57. Sabat KC, Paramguru RK, Mishra BK (2017) Reduction of oxide mixtures of (Fe<sub>2</sub>O<sub>3</sub> + CuO) and (Fe<sub>2</sub>O<sub>3</sub> + Co<sub>3</sub>O<sub>4</sub>) by low-temperature hydrogen plasma. *Plasma Chem Plasma Process* 37:979–995. <https://doi.org/10.1007/s11090-017-9818-6>
58. Sabat KC (2019) Formation of CuCo alloy from their oxide mixtures through reduction by low-temperature hydrogen plasma. *Plasma Chem Plasma Process* 39:1071–1086. <https://doi.org/10.1007/s11090-019-09963-y>
59. Sabat KC, Paramguru RK, Mishra BK (2018) Formation of copper–nickel alloy from their oxide mixtures through reduction by low-temperature hydrogen plasma. *Plasma Chem Plasma Process* 38:621–635. <https://doi.org/10.1007/s11090-018-9880-8>
60. Rajput P, Bhoi B, Paramguru RK, Mishra BK (2016) Effect Of plasma state and alloying addition on reduction of Fe<sub>2</sub>O<sub>3</sub> by a low-temperature hydrogen plasma. *High Temp Mater Process* 20:317–332
61. Sabat KC, Murphy AB (2017) Hydrogen plasma processing of iron ore. *Metall Mater Trans B Process Metall Mater Process Sci* 48:1561–1594. <https://doi.org/10.1007/s11663-017-0957-1>
62. Sabat KC, Paramguru RK, Mishra BK (2016) Reduction of copper oxide by low-temperature hydrogen plasma. *Plasma Chem Plasma Process* 36:1111–1124. <https://doi.org/10.1007/s11090-016-9710-9>
63. Yu X, Zhang X (2017) High coverage water adsorption on CuO(011) surface. *Phys Chem Chem Phys* 19:18652–18659. <https://doi.org/10.1039/c7cp03003g>
64. Dereñ J, Stoch J (1970) Effect of biography on stoichiometric composition and chemisorptive properties of nickel oxide (oxygen chemisorption). *J Catal* 18:249–259. [https://doi.org/10.1016/0021-9517\(70\)90319-2](https://doi.org/10.1016/0021-9517(70)90319-2)
65. Holder CF, Schaak RE (2019) Tutorial on powder X-ray diffraction for characterizing nanoscale materials. *ACS Nano* 13:7359–7365. <https://doi.org/10.1021/acsnano.9b05157>
66. Cullity SR, Stock BD (2001) *Elements of x-ray diffraction*. Prentice Hall, New Jersey
67. Soo Kim D, Chul Lee H (2012) Nickel vacancy behavior in the electrical conductance of nonstoichiometric nickel oxide film. *J Appl Phys* 112(3): 034504. <https://doi.org/10.1063/1.4742993>
68. Dereñ J, Mrowec S (1973) Semiconducting and transport properties of mono- and polycrystalline nickel oxide. *J Mater Sci* 8:545–558. <https://doi.org/10.1007/BF00550459>
69. Bielański A, Dereñ J, Haber J, Stoczyński J (1962) Physico-chemical properties of alkali- and iron-doped nickel oxide. *Trans Faraday Soc* 58:166–175. <https://doi.org/10.1039/TF9625800166>
70. Dereñ J, Nowotny J (1969) Mechanism and kinetics of interaction between gaseous oxygen and nickel oxide surfaces. *Oxid Met* 1:73–91. <https://doi.org/10.1007/BF00609925>
71. Dubey P, Kaurav N, Devan RS et al (2018) The effect of stoichiometry on the structural, thermal and electronic properties of thermally decomposed nickel oxide. *RSC Adv* 8:5882–5890. <https://doi.org/10.1039/c8ra00157j>
72. Payne BP, Biesinger MC, McIntyre NS (2012) Use of oxygen/nickel ratios in the XPS characterisation of oxide phases on nickel metal and nickel alloy surfaces. *J Electron Spectros Relat Phenomena* 185:159–166. <https://doi.org/10.1016/j.elspec.2012.06.008>
73. Payne BP, Biesinger MC, McIntyre NS (2009) The study of polycrystalline nickel metal oxidation by water vapour. *J Electron Spectros Relat Phenomena* 175(1–3):55–65. <https://doi.org/10.1016/j.elspec.2009.07.006>
74. Biesinger MC, Payne BP, Lau LWM et al (2009) X-ray photoelectron spectroscopic chemical state quantification of mixed nickel metal, oxide and hydroxide systems. *Surf Interface Anal* 41:324–332. <https://doi.org/10.1002/sia.3026>

75. Norton PR, Tapping RL, Goodale JW (1977) A photoemission study of the interaction of Ni(100), (110) and (111) surfaces with oxygen. *Surf Sci* 65:13–36. [https://doi.org/10.1016/0039-6028\(77\)90289-8](https://doi.org/10.1016/0039-6028(77)90289-8)
76. Roberts MW, Smart RSC (1984) The defect structure of nickel oxide surfaces as revealed by photoelectron spectroscopy. *J Chem Soc Faraday Trans* 80:2957–2968. <https://doi.org/10.1039/F19848002957>
77. Carley AF, Chalker PR, Roberts MW (1985) Defects in oxide overlayers at nickel single-crystal surfaces. In: *Proceedings of The Royal Society of London, Series A: Mathematical and Physical Sciences*, vol 399, pp 167–179
78. Dubey P, Kaurav N (2017) Synthesis and thermogravimetric analysis of non-stoichiometric nickel oxide compounds. *J Phys Conf Ser*. <https://doi.org/10.1088/1742-6596/836/1/012040>
79. Bielański A (1979) Oxygen in catalysis on transition metal oxides. *Catal Rev* 19:1–41. <https://doi.org/10.1080/03602457908065099>
80. Yin X, Guo Y, Xie H et al (2019) Nickel oxide as efficient hole transport materials for perovskite solar cells. *Sol RRL* 3:1–27. <https://doi.org/10.1002/solr.201900001>
81. Wang Q, Puntambekar A, Chakrapani V (2016) Vacancy-induced semiconductor-insulator-metal transitions in nonstoichiometric nickel and tungsten oxides. *Nano Lett* 16:7067–7077. <https://doi.org/10.1021/acs.nanolett.6b03311>
82. Dubey P, Kaurav N (2019) Stoichiometric and nonstoichiometric compounds. *intechOpen*, London
83. Karsthof R, Anton AM, Kremer F, Grundmann M (2020) Nickel vacancy acceptor in nickel oxide: doping beyond thermodynamic equilibrium. *Phys Rev Mater* 4:1–9. <https://doi.org/10.1103/PhysRevMaterials.4.034601>
84. Hala M, Capek J, Zabeida O et al (2012) Hysteresis-free deposition of niobium oxide films by HiPIMS using different pulse management strategies. *J Phys D Appl Phys* 45:1–28. <https://doi.org/10.1088/0022-3727/45/5/055204>
85. National Institute of Standards and Technology (2012) NIST-JANAF Thermochemical Tables. <https://janaf.nist.gov/>. Accessed 13 Mar 2021
86. Gamsjäger H, Bugajski J, Preis W et al (2005) *Chemical thermodynamics of nickel*. Elsevier Amsterdam, Netherlands
87. Dieke GH (1958) The molecular spectrum of hydrogen and its isotopes. *J Mol Spectrosc* 2:494–517. [https://doi.org/10.1016/0022-2852\(58\)90095-X](https://doi.org/10.1016/0022-2852(58)90095-X)
88. III RDJ NIST Computational Chemistry Comparison and Benchmark Database, NIST Standard Reference Database Number 101 Release 21, August 2020., <https://cccbdb.nist.gov/exp2x.asp?casno=1333740&charge=0>
89. Sabat KC (2022) Hematite reduction by hydrogen plasma: Where are we now? *Int J Miner Metall Mater*. <https://doi.org/10.1007/s12613-022-2467-7>
90. Dey S, Mehta NS (2020) Oxidation of carbon monoxide over various nickel oxide catalysts in different conditions: a review. *Chem Eng J Adv* 1:100008. <https://doi.org/10.1016/j.ceja.2020.100008>
91. Richardson JT, Scates R, Twigg MV (2003) X-ray diffraction study of nickel oxide reduction by hydrogen. *Appl Catal A-General* 246:137–150
92. Szekely J, Evans JW, Sohn HY (1976) *Gas-solid reactions*. Academic Press, London
93. Sohn HY, Wadsworth ME (1979) *Rate processes of extractive metallurgy*, 1st edn. Plenum Press, New York
94. Sohn H (2005) *Fundamentals of Metallurgy*. In: Seetharaman S (ed) Woodhead Publishing Limited, Cambridge. Woodhead Publishing Limited, Cambridge, pp 299–310
95. Seetharaman S (2014) *Treatise on Process Metallurgy*. Treatise on Process Metallurgy, 1st edn. Elsevier, Netherland, pp 1–1810
96. Sohn HY (2020) *Fluid-Solid Reactions*. Elsevier
97. Furstenau RP, McDougall G, Langell MA (1985) Initial stages of hydrogen reduction of NiO(100). *Surf Sci* 150:55–79. [https://doi.org/10.1016/0039-6028\(85\)90211-0](https://doi.org/10.1016/0039-6028(85)90211-0)
98. Shams El Din AM, El Dahshan ME, Taj El Din AM (2000) Dissolution of copper and copper-nickel alloys in aerated dilute HCl solutions. *Desalination* 130:89–97. [https://doi.org/10.1016/S0011-9164\(00\)00077-1](https://doi.org/10.1016/S0011-9164(00)00077-1)
99. Seetharaman S (2005) *Fundamentals of metallurgy*. Elsevier